Equation of state for confined fluids

Vilde Bråten,[1] Daniel Tianhou Zhang,[2] Morten Hammer,[3,4] Ailo Aasen,[4] Sondre Kvalvåg Schnell,[1] and Øivind Wilhelmsen[3,4,a)]

[1)]*Department of Materials Science and Engineering, Norwegian University of Science and Technology, NTNU, Trondheim, NO-7491, Norway*

[2)]*Department of Chemistry, Norwegian University of Science and Technology, NTNU, Trondheim, NO-7491, Norway*

[3)]*Porelab, Department of Chemistry, Norwegian University of Science and Technology, NTNU, Trondheim, NO-7491, Norway*

[4)]*PoreLab, SINTEF Energy Research, Gas Technology, Trondheim, NO-7465, Norway*

(Dated: 25 May 2022)

Fluids confined in small volumes behave differently than fluids in bulk systems. For bulk systems, a compact summary of the system's thermodynamic properties is provided by equations of state. For confined fluids, however, there is currently a lack of successful methods to predict thermodynamic properties by use of equations of state, since the thermodynamic state depends on additional parameters introduced by the enclosing surface. In this work, we present a consistent thermodynamic framework that represents an equation of state for pure, confined fluids. The total system is decomposed into a bulk phase in equilibrium with a surface phase. The equation of state is based on an existing, accurate description of the bulk fluid, and uses Gibbs' framework for surface excess properties to consistently incorporate contributions from the surface. We apply the equation of state to a Lennard-Jones spline fluid confined by a spherical surface with a Weeks-Chandler-Andersen wall-potential. The pressure and internal energy predicted from the equation of state are nearly within the accuracy of properties obtained directly from molecular dynamics simulations. We find that when the location of the dividing surface is chosen appropriately, the properties of highly curved surfaces can be predicted from those of a planar surface. The choice of dividing surface affects the magnitude of the surface excess properties and their curvature dependence, but the properties of the total system remain unchanged. The framework can predict the properties of confined systems with a wide range of geometries, sizes, inter-particle interactions and wall-particle interactions, and it is independent of ensemble. A targeted area of use is prediction of thermodynamic properties in porous media, for which a possible application of the framework is elaborated.

I. INTRODUCTION

The behavior of fluids is known to change when confined in small geometries. In porous materials for instance, a liquid-phase can form through capillary condensation at pressures below the saturation pressure.[1–4] A popular example in the literature is confined water, where changes in both the dynamic behavior and phase transitions have been observed.[5–7] Molecular dynamics (MD) and Monte Carlo simulations, as well as density functional theory are popular tools that have been used with great success to gain insight into how the fluid behavior is influenced by confinement.[8–13] There is, however, a need for a compact and predictive thermodynamic description of confined fluids that can be used to shed further light on the intriguing findings from simulations.

Equations of state (EoS) provide a compact summary of a system's thermodynamic properties. For homogeneous fluids in macroscopic systems, the temperature, mass density and composition are usually sufficient to characterize the thermodynamic state of the fluid. In confined systems, additional knowledge about features such as the system's geometry and wall-fluid interactions are needed since this can lead to wall-adsorption, layering and disjoining effects.[8–11] For simple systems, such as ideal gas systems[14] or systems containing a small number of particles,[15] the effects of confinement can be included in exact expressions for the thermodynamic properties. For fluids with interacting particles, cubic EoS are popular tools that have been used extensively in process simulations, optimization studies, and solubility predictions.[16,17] There have been some efforts to develop cubic EoS for confined systems. Zarragoicoechea and Kuz[18] derived the van der Waals (vdW) EoS for a square-section nano-pore of infinite length[18] that predicted a shift in the critical point.[19] Travalloni *et al.* later introduced wall-fluid interactions to the vdW EoS.[20,21]

One major challenge in the development of cubic EoS for confined systems is that experimental characterization of fluids in nano-geometries is difficult. Challenges associated with validation of the EoS is an issue for all types of EoS that depend on parameters obtained from experiments.[22] Instead of parametrizing the experimental properties of confined fluids, it can therefore be advantageous to base the EoS on fluids described by interaction potentials. This makes it possible to test the EoS predictions by comparing them to properties computed directly from molecular simulations in well-defined geometries. For instance, the thermodynamic properties of the hard-sphere fluid in a random porous medium have been successfully represented by scaled particle theory.[23] This description has later been applied in investigations of the properties of various fluids confined in a random porous media, such as the Lennard-Jones (LJ) fluid,[24] a poly-disperse square-well chain fluid[25] and a fluid of particles interacting through a hard-sphere Morse potential.[26]

In this work, we formulate a general thermodynamic de-

[a)]Electronic mail: oivind.wilhelmsen@ntnu.no

scription that applies to fluids of a wide variety of interparticle interactions confined in systems with a wide range of wall-fluid interactions, geometries and sizes. Since the EoS should return to the bulk description when the system is large enough, we base the EoS on an existing bulk description and show how surface contributions can be incorporated into the description. The surface contributions arise from the interactions between the fluid and the enclosing surface, which become increasingly relevant as the number of particles and volume decrease. A consequence of this is that, for sufficiently small systems, properties that are extensive in macroscopic systems are no longer Euler homogeneous of degree one.[27] The nanothermodynamic framework developed by Hill[28] is a consistent extension of classical thermodynamics that can be applied to such systems. Nanothermodynamics has been used in various efforts to understand the behavior of small systems, like stretching and breaking of polymer chains[29,30] and transport in porous media.[31–33] In addition, nanothermodynamics has supported the analysis of size-scaling of thermodynamic properties, which is crucial for computation of macroscopic properties from sub-sampling techniques.[34–36] In order to use Hill's[28] framework to gain insight on the behavior of small systems, the underlying physical description of the system is required. In this work, we derive such a physical description by employing the framework of excess variables developed by Gibbs.[37] We split the thermodynamic description of a small system into a bulk phase and an excess, small-size contribution. The leading order small-size contribution usually comes from the system's surface area. We emphasize that line- and edge-contributions could also be relevant[38,39], but they are beyond the scope of the present work. For system sizes where the total confined system can be described as a bulk phase and its excess surface phase, the formalism presented here provides a consistent framework that represents an EoS for confined systems. In particular, we show that the EoS reproduces results from molecular simulations of confined fluids nearly within the simulation accuracy.

II. THEORETICAL FRAMEWORK

In this section, we present a thermodynamic framework to describe confined fluids. The thermodynamic description of the system is split into a bulk phase and an excess surface phase. We consider the case where there is local equilibrium in both the bulk phase and the surface phase. In the following, properties with no subscript refer to the total system, properties with subscript "b" refer to the bulk phase, while properties with subscript "s" refer to the excess surface phase. We formulate the internal energy, U, as a function of the entropy, S, number of particles, N, and volume, V, for the bulk phase or area, Ω, for the surface phase. The volume of the total system is defined as the bulk volume, $V = V_\mathrm{b}$, and the area of the total system is defined as the surface phase area, $\Omega = \Omega_\mathrm{s}$. The entropy, number of particles and internal energy are split into a bulk contribution and an excess surface contribution as follows

$$N = N_\mathrm{b} + N_\mathrm{s} = N_\mathrm{b} + \Gamma\Omega, \tag{1}$$

$$S = S_\mathrm{b} + S_\mathrm{s} = S_\mathrm{b} + \eta\Omega, \tag{2}$$

$$U(N,V,S) = U_\mathrm{b}(N_\mathrm{b},V,S_\mathrm{b}) + U_\mathrm{s}(N_\mathrm{s},\Omega,S_\mathrm{s}), \tag{3}$$

where Γ is the excess number of particles per area, which is also referred to as the adsorption, and η is the excess entropy per area. The surface phase described by excess variables is an autonomous thermodynamic system. This means that the surface phase has its own temperature, T_s, and chemical potential, μ_s. When the bulk phase is not in equilibrium with the surface phase, the bulk temperature, T_b, and the bulk chemical potential, μ_b, can differ from those of the surface phase. This leads to the following expressions for the internal energy of the bulk phase

$$U_\mathrm{b} = T_\mathrm{b}S_\mathrm{b} - p_\mathrm{b}V + \mu_\mathrm{b}N_\mathrm{b}, \tag{4}$$

and the internal energy of the surface phase

$$U_\mathrm{s} = T_\mathrm{s}S_\mathrm{s} + \gamma\Omega + \mu_\mathrm{s}N_\mathrm{s}, \tag{5}$$

where p is the pressure and γ is the surface energy.

In the following, we consider the situation where the bulk phase is in equilibrium with the surface phase, meaning that $T_\mathrm{b} = T_\mathrm{s}$ and $\mu_\mathrm{b} = \mu_\mathrm{s}$. Under these circumstances, we define the pressure and chemical potential in the system as

$$p \equiv p_\mathrm{b} = -\left(\frac{\partial U_\mathrm{b}}{\partial V}\right)_{N_\mathrm{b},S_\mathrm{b}}, \tag{6}$$

$$\mu \equiv \mu_\mathrm{b} = \left(\frac{\partial U_\mathrm{b}}{\partial N_\mathrm{b}}\right)_{V,S_\mathrm{b}}, \tag{7}$$

and the internal energy of the total confined system becomes

$$U = TS - pV + \mu N + \gamma\Omega. \tag{8}$$

A central quantity for the framework presented in this work is the bulk density

$$\rho_\mathrm{b} = \frac{N_\mathrm{b}}{V} = \frac{N - \Gamma\Omega}{V}, \tag{9}$$

which for confined systems usually differs from the total density, $\rho = N/V$.

A key advantage with the formulation above is that intensive properties of the total confined system can be determined by considering the properties of the bulk phase as a function of T and ρ_b. In the formalism presented in this work, the bulk density can be computed from Eq. (9) when the total number of particles, the adsorption and the system's geometry are known. To determine the total entropy and the total internal energy of the confined fluid one also needs the excess entropy and the surface energy.

We shall hereby refer to the framework for computation of the properties of confined fluids as the "Nano-EoS". In Sec. II A, we explain how the properties of the bulk phase of the confined fluid can be computed from a bulk-EoS. In Sec. II B, we explain how the properties of the surface phase

of a confined fluid in equilibrium can be computed when the adsorption is known. This "developer perspective" is demonstrated in Sec. IV for a Lennard-Jones spline fluid confined in a spherical container. In Sec. V, we demonstrate the "user perspective" by applying the Nano-EoS in the way a future user would, i.e. extracting the thermodynamic properties with only T, ρ_b and geometry variables as input. All thermodynamic properties computed from either the Nano-EoS or the bulk-EoS have superscript "EoS".

The Nano-EoS presented in this work is independent of ensemble since $U_\mathrm{b}(N_\mathrm{b},V,S_\mathrm{b})$ and $U_\mathrm{s}(N_\mathrm{s},\Omega,S_\mathrm{s})$ are both Euler homogeneous of degree one. The energy state functions for various ensembles are therefore accessible from Legendre transformations of the internal energy of each phase. Ensemble dependence has been observed for both the pressure and the chemical potential in small systems.[14] However, we do not consider ensemble effects here since, for the system types we investigate, the Nano-EoS is expected to break down at system sizes larger than those where ensemble effects are relevant. See Bråten *et al.*[14] for a detailed discussion of when ensemble dependence becomes relevant.

A. Bulk properties

For a given bulk density, the properties of the bulk phase can be extracted from a bulk-EoS. The bulk internal energy is therefore

$$U_\mathrm{b}^\mathrm{EoS} = U_\mathrm{b}^\mathrm{EoS}(N_\mathrm{b},V,T). \tag{10}$$

Other properties of the bulk phase, such as energy state functions or entropy, can be computed from equivalent relations. Note that the internal energy extracted from a bulk-EoS often is normalized by the number of particles $U_\mathrm{b}^\mathrm{EoS}(N_\mathrm{b},V,T)/N_\mathrm{b}$. The bulk internal energy of the confined system is therefore computed by multiplying the bulk prediction with N_b.

B. Surface excess properties

A prerequisite for computing surface excess properties is to define the location of the dividing surface. There are many different choices available, and the location of the dividing surface determines the value of V, and for curved surfaces it also affects Ω. The choice of dividing surface influences the decomposition into bulk and surface contributions. Some properties are invariant to the choice of dividing surface, such as the total internal energy of the confined fluid. Details on how the surface excess properties for different choices of dividing surface are related to each other are presented in Sec. II B 2.

The surface phase is the excess with respect to a bulk phase at ρ_b and T. For equilibrium systems, the surface excess properties are therefore considered as functions of these two variables. Our starting point for computation of surface excess properties is the adsorption, which is computed from

$$\Gamma = \frac{N-\rho_\mathrm{b}V}{\Omega}. \tag{11}$$

The adsorption is related to the other surface excess properties and the intensive properties of the total system through Gibbs adsorption equation.[37] For a given choice of dividing surface at a fixed position relative to the total volume, Gibbs adsorption equation is

$$\mathrm{d}\gamma = -\Gamma\mathrm{d}\mu - \eta\mathrm{d}T. \tag{12}$$

At constant temperature, Eq. (12) becomes

$$\mathrm{d}\gamma = -\Gamma\mathrm{d}\mu. \tag{13}$$

When the adsorption and the chemical potential is known for a range of different bulk densities, Eq. (13) can be used to compute the differential surface energy. By using that the surface energy is zero at zero density, the absolute value of the surface energy can be computed.

At constant chemical potential, Eq. (12) can be rewritten as an expression for the excess entropy per area

$$\eta = -\left.\frac{\partial\gamma}{\partial T}\right|_\mu. \tag{14}$$

From Eq. (14) it is apparent that η as a function of bulk density can be readily computed from the temperature dependence of the surface energy when one knows how the chemical potential depends on the bulk density and the temperature.

The excess internal energy becomes

$$U_\mathrm{s}^\mathrm{EoS} = T\eta\Omega + \gamma\Omega + \mu\Gamma\Omega. \tag{15}$$

1. Curvature dependence of surface properties

The surface excess properties depend on the geometry of the surface. For non-planar surfaces, the surface properties can be expressed as the surface properties of a planar wall plus additional curvature corrections.[38,39] The adsorption for a spherical surface with radius R is expressed as

$$\Gamma(R) = \Gamma_0 + \frac{\Gamma_1}{R} + \mathscr{O}\left(\frac{1}{R^2}\right), \tag{16}$$

where Γ_0 refers to the adsorption at a planar wall, Γ_1 is the first-order curvature correction to the adsorption and $\mathscr{O}\left(1/R^2\right)$ refers to the higher order terms. Both the surface energy and the excess entropy per area can be expressed by equations similar to Eq. (16), and become

$$\gamma(R) = \gamma_0 + \frac{\gamma_1}{R} + \mathscr{O}\left(\frac{1}{R^2}\right), \tag{17}$$

$$\eta(R) = \eta_0 + \frac{\eta_1}{R} + \mathscr{O}\left(\frac{1}{R^2}\right). \tag{18}$$

In this work, we only investigate the first-order corrections, but higher order corrections are also possible.[40,41] For the systems considered here, R is independent of T and μ. This means that γ_0 and γ_1 can be computed from Eq. (13) when Γ_0 and Γ_1 are known, and that η_0 and η_1 can be computed from Eq. (14) when γ_0 and γ_1 are known.

The capillary approximation (CA) states that the surface properties of a curved surface are equal to those of a planar surface. When the curvature corrections are small compared to the planar-wall contribution, the capillary approximation may provide a satisfactory description of the surface excess properties. In Sec. V, we discuss when the capillary approximation holds for confined fluids.

2. Shifting the location of the dividing surface

For the system types we consider, the volume of the system depends on the location of the dividing surface. Consequently, Γ, η and γ will also depend on the location of the dividing surface.[40,42] In this section, we show how the surface properties of one dividing surface are related to those of another dividing surface.

In simulations, the fluid particles are confined by a wall. For spherical systems, this wall is located at the enclosing surface, $\widetilde{\Omega}$, at a distance $\widetilde{R}$ from the center of the sphere. This enclosing surface corresponds to the volume $\widetilde{V}$. For a box-shaped system, with a wall located at one of the sides, the surface area of this wall is independent of the dividing surface, $\widetilde{\Omega} = \Omega$, and the volume defined by the location of the wall is $\widetilde{V} = \widetilde{L}\Omega$. The location of the dividing surface can be specified as the distance from the enclosing wall, d_{wall}, which will be called to as the wall-thickness. Its sign is as positive when $V < \tilde{V}$, cf. Fig. 1. For a wall-thickness $d_{\text{wall}} = 0$, the volume and area corresponding to the dividing surface are $\widetilde{V}$ and $\widetilde{\Omega}$. Surface excess properties computed for this choice of dividing surface are marked by a tilde.

For some expressions for surface excess properties, a dividing surface located at $d_{\text{wall}} = 0$ is implicit for the system types investigated in this work. These are the excess functions for the adsorption and the excess entropy, and the surface energy computed from the Kirkwood-Buff[43] (KB) equation. The respective excess functions for the adsorption and the excess entropy are

$$\widetilde{\Gamma} = \frac{1}{\widetilde{\Omega}} \int [\rho(\xi) - \rho_{\text{b}}] \, \mathrm{d}\widetilde{V}, \tag{19}$$

$$\widetilde{\eta} = \frac{1}{\widetilde{\Omega}} \int [s(\xi) - s_{\text{b}}] \, \mathrm{d}\widetilde{V}, \tag{20}$$

where ξ is the coordinate normal to the wall, $\rho(\xi)$ is the number density profile, $s(\xi)$ is the entropy density profile and s_{b} is the bulk entropy density. The KB equation utilizes the pressure anisotropy close to the surface, and relates the surface energy to the pressure tensor profiles. For a box-shaped system, the surface energy can be computed from the KB equation

$$\widetilde{\gamma} = \int_0^{\widetilde{L}} [p_N(\xi) - p_T(\xi)] \, \mathrm{d}\xi, \tag{21}$$

where p_N and p_T are the normal and tangential components of the pressure tensor respectively. The normal component of the pressure tensor is equal to the bulk pressure, $p_N(\xi) = p_{\text{b}}$[32]. The KB equation can also be defined for curved surfaces, but correct computation of pressure tensors in vicinity of curved surfaces remains an unresolved topic.[11,44–47]

The surface properties for $d_{\text{wall}} = 0$ are related to the surface properties for a dividing surface located at $d_{\text{wall}} \neq 0$. For a planar wall, these relations are

$$\widetilde{\Gamma_0} - \Gamma_0 = -\rho_{\text{b}} d_{\text{wall}}, \tag{22}$$

$$\widetilde{\gamma_0} - \gamma_0 = p_{\text{b}} d_{\text{wall}}, \tag{23}$$

$$\widetilde{\eta_0} - \eta_0 = -s_{\text{b}} d_{\text{wall}}, \tag{24}$$

and the relations for the curvature corrections of a spherical surface are

$$\widetilde{\Gamma_1} - \Gamma_1 = \rho_{\text{b}} d_{\text{wall}}^2 - 2 d_{\text{wall}} \Gamma_0, \tag{25}$$

$$\widetilde{\gamma_1} - \gamma_1 = -p_{\text{b}} d_{\text{wall}}^2 - 2 d_{\text{wall}} \gamma_0, \tag{26}$$

$$\widetilde{\eta_1} - \eta_1 = s_{\text{b}} d_{\text{wall}}^2 - 2 d_{\text{wall}} \eta_0, . \tag{27}$$

Equations (22)-(26) provide general relations between the surface excess properties for two dividing surfaces separated by a distance d_{wall}. In this work, we apply them to the specific case where where $\widetilde{\Gamma}$, $\widetilde{\gamma}$ and $\widetilde{\eta}$ correspond to a dividing surface located at $d_{\text{wall}} = 0$. Further details about the derivation of Eqs. (22)-(26) are given in the supplementary material.

3. Surface properties in the low-density limit

For low-density systems, computation of statistical averages from molecular simulations requires considerable computational effort. Exact analytical expressions that provide a consistent description of the system's properties at low densities are therefore useful. In the low-density limit, the properties of fluids with interacting particles can be approximated by the properties of an ideal gas. In this section, we show how the surface excess properties of a confined ideal gas can be computed analytically.

The ideal gas particles do not interact with each other, but they do interact with the enclosing wall. The interaction energy between the particles and the wall is given by the wall-potential $W(\xi)$. In the region where the wall-potential is zero, the potential energy of the system is zero, and the density is equal to the bulk density. The density profile for the coordinate normal to the wall is[48]

$$\rho_{\text{IG}}(\xi) = \rho_{\text{b}} \exp\left(-\frac{W(\xi)}{k_{\text{B}}T}\right). \tag{28}$$

Combining Eq. (28) with Eq. (19) yields the expression for the adsorption of an ideal gas

$$\begin{aligned} \widetilde{\Gamma_{\text{IG}}} &= \frac{1}{\widetilde{\Omega}} \int [\rho_{\text{IG}}(\xi) - \rho_{\text{b}}] \, \mathrm{d}\widetilde{V} \\ &= \rho_{\text{b}} \frac{1}{\widetilde{\Omega}} \int \left[\exp\left(-\frac{W(\xi)}{k_{\text{B}}T}\right) - 1\right] \mathrm{d}\widetilde{V}. \end{aligned} \tag{29}$$

Since the integral in the above expression is independent of density, the adsorption becomes a first-order linear function of the bulk density, where the slope is

$$\widetilde{\alpha} = \frac{1}{\widetilde{\Omega}} \int \left[\exp\left(-\frac{W(\xi)}{k_{\text{B}}T}\right) - 1\right] \mathrm{d}\widetilde{V}. \tag{30}$$

This slope depends on the temperature and the geometry of the system, but it is independent of the bulk density. The differential of $\widetilde{\alpha}$ with respect to temperature is

$$\frac{\mathrm{d}\widetilde{\alpha}}{\mathrm{d}T} = \frac{1}{\widetilde{\Omega}} \int \exp\left(-\frac{W(\xi)}{k_\mathrm{B}T}\right) \frac{W(\xi)}{k_\mathrm{B}T^2} \mathrm{d}\tilde{V}. \tag{31}$$

Further details about computation of α for different choices of dividing surface are presented in the supplementary material.

The following equations are valid for any choice of dividing surface and we therefore omit the tilde. The adsorption of the confined ideal gas is

$$\Gamma_\mathrm{IG} = \alpha\rho_\mathrm{b}, \tag{32}$$

and the surface energy can be obtained from Gibbs adsorption equation at constant temperature

$$\mathrm{d}\gamma_\mathrm{IG} = -\Gamma_\mathrm{IG}\mathrm{d}\mu_\mathrm{IG}, \tag{33}$$

The integration variable μ_IG can be substituted for ρ_b through the expression for the chemical potential of an ideal gas

$$\mu_\mathrm{IG} = k_\mathrm{B}T \ln\left(\frac{\rho_\mathrm{b}k_\mathrm{B}T}{p_0}\right) + \mu_0(T), \tag{34}$$

where p_0 is the pressure of the standard state and μ_0 is the reference chemical potential. More details on choice of reference state are presented in the supplementary material. The differential chemical potential at constant temperaure becomes $\mathrm{d}\mu_\mathrm{IG} = k_\mathrm{B}T\rho_\mathrm{b}^{-1}\mathrm{d}\rho_\mathrm{b}$, and since the surface energy is zero at zero density, integration of Eq. (33) yields

$$\gamma_\mathrm{IG} = -k_\mathrm{B}T\alpha\rho_\mathrm{b}. \tag{35}$$

Similar to the adsorption, the surface energy of the ideal gas is a first-order linear function of ρ_b. This implies the simple relationship: $\gamma_\mathrm{IG} = -k_\mathrm{B}T\Gamma_\mathrm{IG}$.

The excess entropy of the confined ideal gas is computed from the Gibbs adsorption equation at constant chemical potential, presented in Eq. (14). Differentiating the surface energy of the ideal gas with respect to temperature at constant chemical potential yields

$$\begin{aligned}\eta_\mathrm{IG} = -\left.\frac{\partial\gamma_\mathrm{IG}}{\partial T}\right|_{\mu_\mathrm{IG}} &= \rho_\mathrm{b}\left(k_\mathrm{B}T\frac{\mathrm{d}\alpha}{\mathrm{d}T} - \alpha\frac{\mathrm{d}\mu_0}{\mathrm{d}T}\right) \\ &\quad -k_\mathrm{B}\alpha\rho_\mathrm{b}\ln\left(\frac{\rho_\mathrm{b}k_\mathrm{B}T}{p_0}\right).\end{aligned} \tag{36}$$

In contrast to the adsorption and the surface energy, the excess entropy is not a first-order linear function of the bulk density. The excess entropy for a confined ideal gas consists of one term that is linear in ρ_b and one term that contains the nonlinearity $\rho_\mathrm{b}\ln(\rho_\mathrm{b}k_\mathrm{B}T/p_0)$. The last term comes from the nonlinear relation between the density and the chemical potential.

III. COMPUTATIONAL DETAILS

We compute the thermodynamic properties of a confined fluid directly from MD simulations. This includes the properties of the total system, the bulk phase and the surface phase. To investigate the impact of curvature on the surface excess properties, we compute the values for systems with a planar wall and in spherical systems. In the following, all presented values and results are given in reduced LJ units.

A. Simulation details

The MD simulations are performed with the simulation package LAMMPS.[49] The LAMMPS simulation input files are openly available with download details given in the data availability statement. For the inter-particle interactions, we employ the Lennard-Jones spline (LJs) potential.[50] See Hafskjold *et al.*[51] for a detailed discussion on the properties of systems containing particles interacting via the LJs potential. The interactions between the fluid and the wall are described by the Weeks-Chandler-Andersen (WCA) potential.[52] The WCA potential is a purely repulsive potential that is equal to the LJ potential truncated and shifted at $r_c = 2^{1/6}\sigma_\mathrm{wall}$, where we use $\sigma_\mathrm{wall} = 1$. The volume of the simulation box is $\widetilde{V}$, which is defined by the location of the walls. We consider one system with planar walls with dimensions $\widetilde{V} = \widetilde{L_x}L_yL_z$, where $\widetilde{L_x} = 40$ and $L_y = L_z = 20$, and three differently sized spherical systems with radius $\widetilde{R} = 5, 10, 15$. The spherical systems have a WCA-wall located at $\widetilde{R}$. The system with planar walls have a WCA-wall located at each end of $\widetilde{L_x}$ and periodic boundary conditions in the other directions. Both system types are illustrated in Fig. 1. For all systems, we investigate values of $N/\widetilde{V}$ ranging from 0.05 to 0.80. The simulations are run in five parallels, which consist of 20 million time steps each for $N/\widetilde{V} \leq 0.45$, and 2 million time steps each for $N/\widetilde{V} > 0.45$. The size of the time step is $\Delta t = 0.002$. All densities, geometries and sizes are investigated for five different temperatures, $T = 1.90, 1.95, 2.00, 2.05, 2.10$. The pressure is computed from the virial expression.

B. Bulk equation of state

The bulk equation of state for the LJs fluid used in this work is the *uv*-theory of van Westen and Gross,[53,54] accessed through the open-source thermodynamic software Thermopack.[22,55]

C. Application of the Nano-EoS

The flowchart presented in Fig. 2. explains the procedure for computing thermodynamic properties of a confined fluid when N, T, the fluid's bulk properties and the surface excess properties are known. The procedure shown in the figure can be used to predict the properties of confined fluids at equilibrium.

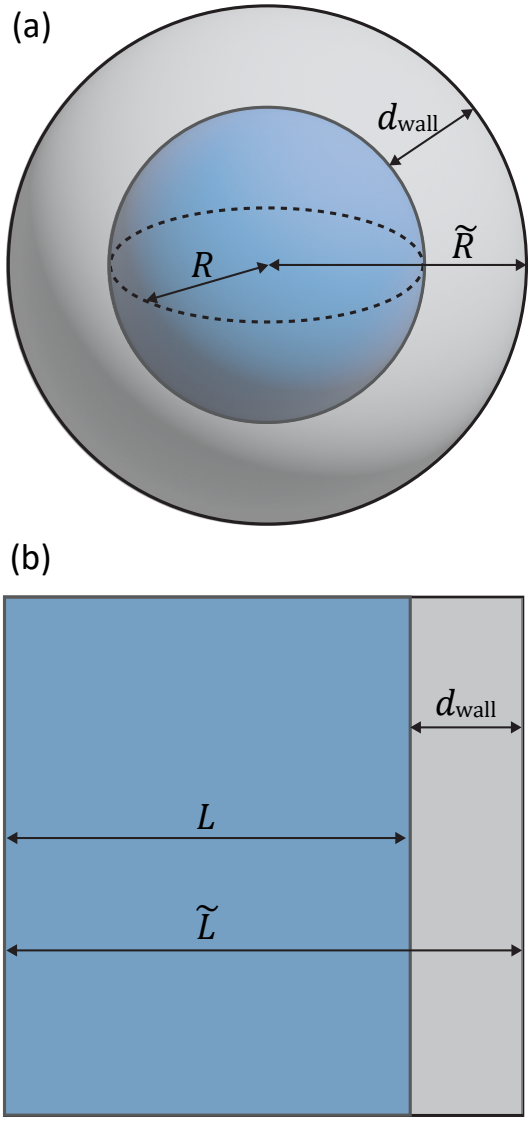

FIG. 1. Illustrations of (a) the spherical system and (b) a cross section of the planar-wall system investigated in this work. The dividing surface is located at R for the spherical system and at L for the planar-wall system, while the WCA-wall is located at $\widetilde{R}$ for the spherical system and at $\widetilde{L}$ for the planar-wall system. The wall-thickness, d_{wall}, is the distance between the dividing surface and the wall. (b) illustrates the section between $\widetilde{L}_x/2$ and $\widetilde{L}_x$ of the system investigated by MD simulations, which means that $\widetilde{L}$ in the figure corresponds to $\widetilde{L}_x/2$ in the simulations.

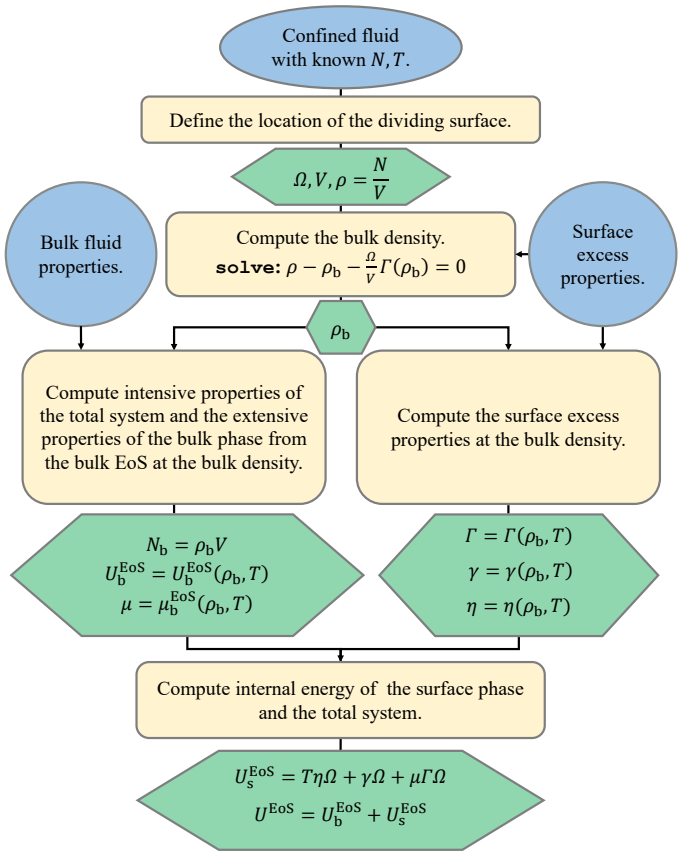

FIG. 2. Flowchart for computing thermodynamic properties of a confined fluid when N, T, the fluid's bulk properties and the surface excess properties are known. The initial input is shown in the blue circles, explanations for each computation step are presented in the yellow boxes and the computed properties are shown in the green hexagons.

IV. RESULTS - MOLECULAR SIMULATIONS OF CONFINED FLUIDS

In this section, we present the step-by-step procedure used for computation and parametrization of the surface excess properties. This represents the "developer perspective". When the surface excess properties are computed and parametrized, they can be utilized to predict thermodynamic properties of systems of any density within the range of validity of the Nano-EoS by following the procedure presented in Fig. 2. This represents the "user perspective", which is demonstrated in Sec. V. The presented results have been computed using a wall-thickness $d_{\text{wall}} = 1$. In the presentation of the results, the sphere sizes are referred to by the radius given by the location of the wall, $\widetilde{R}$. In Sec. VI A, we discuss how the choice of dividing surface impacts the computation of thermodynamic properties from the Nano-EoS. Error bars corresponding to two standard deviations are included in Figs. 4-5, 8 and 13-16.

A. Computation of the bulk properties from simulations

To compute bulk properties from molecular simulations, one needs the location of the bulk region. The *bulk region* is here defined as the region of the system where the local contributions from the wall are negligible, e.g. that thermodynamic properties like the density and the pressure are locally isotropic. When the location of the bulk region is known, the bulk number density, bulk internal energy density and pressure are easily computed from molecular simulations. Note

that the *bulk region* in simulations is not the same as the *bulk phase* in the Nano-EoS. The properties of the bulk phase in the Nano-EoS framework are equal to the properties in the bulk region extrapolated to the entire system volume.

The limits of the bulk region are identified from the system's density profiles. Figure 3 shows the density profiles in the x-direction for the system with planar walls and in the r-direction for the spherical systems. All systems show oscillatory profiles close to the wall that become more distinct with increasing density. The oscillatory behavior is due to structural changes close to the wall, which depend on the type of confinement, the type of fluid and the size of the system.[33,56,57]

For the system with planar walls, the density profiles are all uniform for $20 < x < 30$, which makes it possible to identify one common bulk region for all the different total densities. This is not possible for the spherical systems, since they do not always have a well-defined bulk region. For the spherical systems, the limits of the bulk region are therefore defined individually for each of the total densities investigated. The limits of the bulk regions are displayed by the dashed lines in Fig. 3. In computation of bulk density, bulk pressure and bulk energy density, the data points in the region $r \leq 1$ are discarded due to the large degree of noise. While validation of the Nano-EoS requires a bulk region, we will show in Sec. V that its predictions extrapolate very well beyond this regime. The parametrization of the surface excess properties presented in Sec. IV B thereby allows us to compute the bulk and surface properties of systems that do not have well defined bulk regions.

B. Computation of the surface excess properties from simulations

Surface properties are computed using the formalism presented in Sec. II B. For better readability, the surface properties are only presented for $T = 1.9, 2.0, 2.1$. Equations (32), (35) and (36) show that the adsorption and the surface energy do not depend on the reference state while the excess entropy does depend on the reference state.

In order to extract the surface excess properties at arbitrary densities, all the surface excess properties must be parametrized. For the adsorption and the surface energy, we use 5th and 9th degree polynomials respectively. For the excess entropy, we use a 9th degree polynomial plus the non-linear term $\rho_b \ln(\rho_b k_B T/p_0)$ multiplied with a constant coefficient. The constant term is set to zero for all polynomials in order to ensure that all surface excess properties are zero at zero density. At low densities, the first-order coefficients of the polynomials will dominate, such that the surface properties of the LJs fluid can be approximated by those of the ideal gas presented in Sec. II B 3. In the fitting process, the first-order coefficients are therefore set to the predictions provided by the ideal gas model. The first-order coefficients of the adsorption and the surface energy curves are given by Eqs. (32) and (35) respectively. For the excess entropy curve, both the first-order coefficient and the coefficient of the non-linear term are given by Eq. (36). The coefficients for the parametrized curves of all the surface excess properties are available in the supplementary material.

1. Surface properties of a planar wall

The adsorption is computed from Eq. (11) by combining the bulk densities identified in Sec. IV A and the total densities computed using the volume defined by the dividing surface. Figure 4 shows the adsorption as a function of bulk density, where the fitted curves are displayed by the full lines. The adsorption for purely repulsive walls in contact with fluids interacting through potentials containing both attractive and repulsive parts have previously been studied in detail.[8,11,56] For such systems, the adsorption at low densities is governed by the attractive inter-particle interactions, which favor accumulation of the particles in the bulk region. At higher densities, the repulsive interactions dominate, which favor accumulation of the particles at the wall since this minimizes each particle's excluded volume. We emphasize that the values of the surface excess properties depend on the location of the dividing surface. Whether the computed adsorption curves reflect the above described behavior therefore depends on the choice of dividing surface. Figure 4 shows that a dividing surface at $d_{\text{wall}} = 1$ reflects this behavior since the adsorption is negative at low densities and positive at higher densities for all investigated temperatures.

When the parametrized adsorption is known as a function of bulk density, the surface energy can be computed from Gibbs adsorption equation (Eq. (13)). The surface energy is also computed from the KB equation (Eq. (21)), combined with Eq. (23) in order to extract the surface energy for a dividing surface at $d_{\text{wall}} = 1$. Figure 5 shows the surface energies computed from Gibbs adsorption equation and from the KB equation. With the exception of the data points at the two highest densities, the prediction of the surface energy from Gibbs adsorption equation are within two standard deviations of the value computed using the KB equation. The increased deviation between the two methods observed at higher densities probably arises from numerical integration of Gibbs adsorption. This can be due to inaccuracies in the parametrized adsorption or the bulk chemical potential predicted from the bulk-EoS. The black dotted lines show the curves fitted to the surface energies computed from Gibbs adsorption equation. In the Nano-EoS, we use the surface energies computed from Gibbs adsorption equation, since computing all the surface excess properties with the adsorption as a starting point results in a more consistent framework. Comparison to the surface energies computed from the KB equation works as a quality check for the surface energies computed from Gibbs adsorption equation.

As shown in Eq. (14), the excess entropy is related to the temperature dependence of the surface energy at constant chemical potential. For most fluids, the relation between the chemical potential and density is temperature dependent. We therefore use the bulk-EoS to extract the bulk densities at different temperatures corresponding to a constant chemical po-

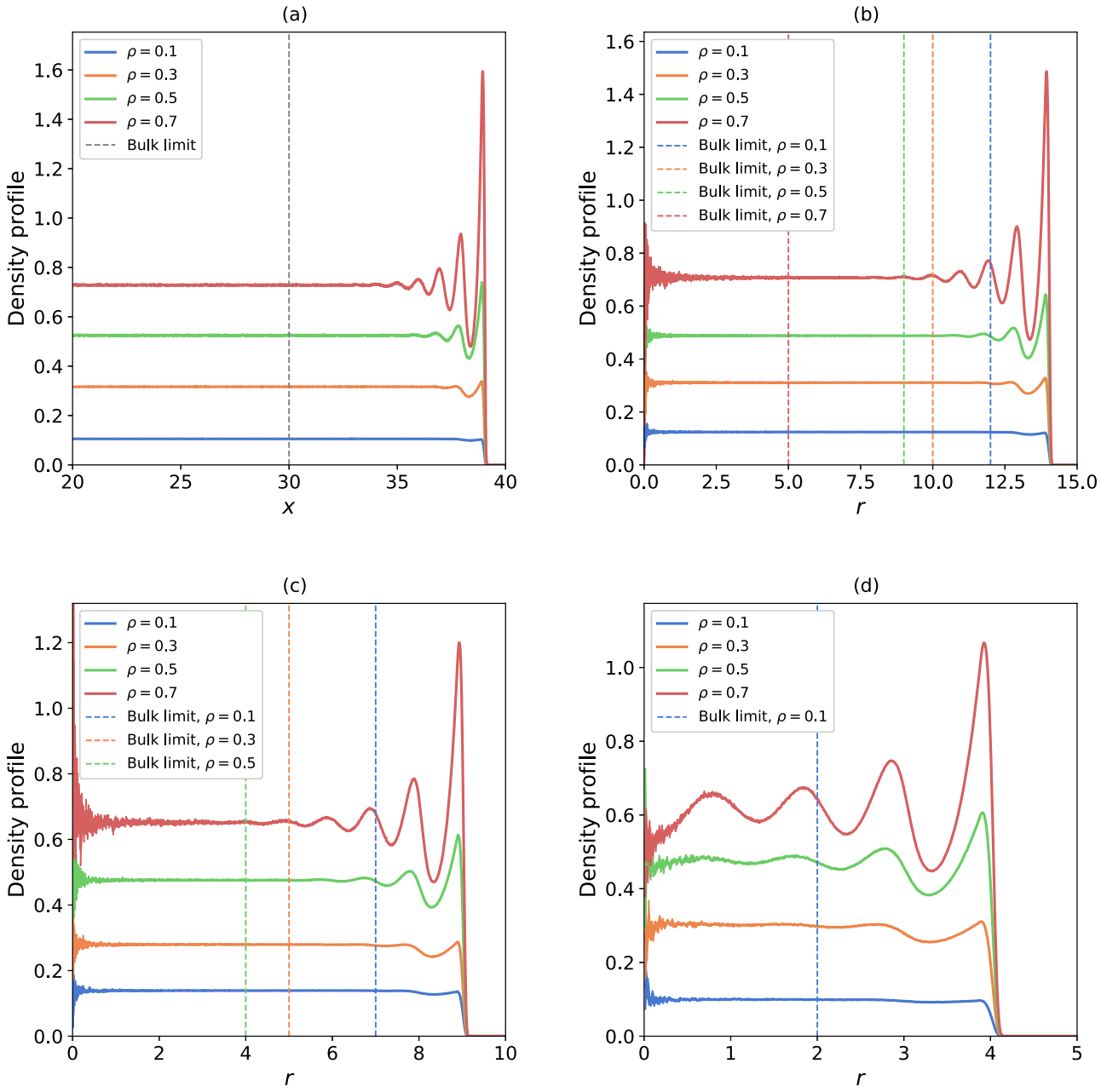

FIG. 3. Density profiles for for a few selected total densities for a (a) planar wall and spherical systems with (b) $\widetilde{R} = 15$ (c) $\widetilde{R} = 10$ (d) $\widetilde{R} = 5$, for $T = 2.0$. Since the planar-wall system is symmetrical around the center of the simulation box, the figure displays the average of the two symmetrical parts. The left side of the profiles of the spherical systems corresponds to the smallest spherical bins in the center of the simulation box.

tential. The surface energies at these densities are extracted from the surface energy polynomial, since these states are not represented by the discrete data points computed directly from simulations. Figure 6 shows the surface energies as functions of the temperature for a few selected chemical potentials. For the small temperature range considered here, the surface energy can be approximated as a first-order linear function of the temperature. This means that the excess entropy at $T = 2.0$ can be extracted from the negative slope of the dashed lines in Fig. 6. The resulting excess entropy as a function of bulk density is displayed in Fig. 7 where the dotted black line is the curve fitted to the excess entropy computed from Eq. (14).

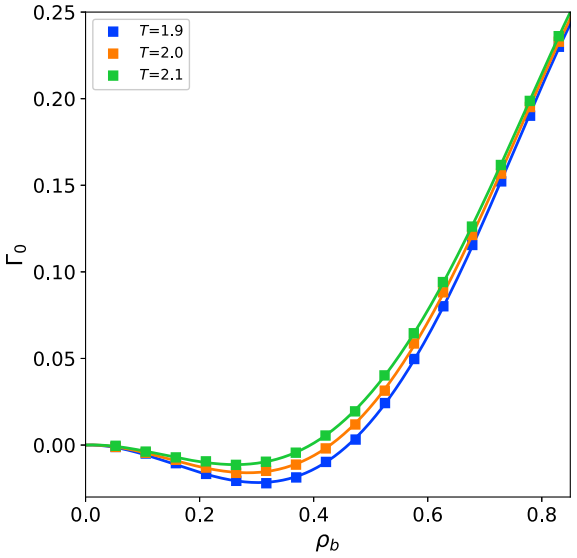

FIG. 4. Adsorption as a function of bulk density for the LJs fluid in contact with a planar wall with a WCA wall-potential. The fitted curves are displayed by the full lines. The dividing surface is located at $d_{\text{wall}} = 1$.

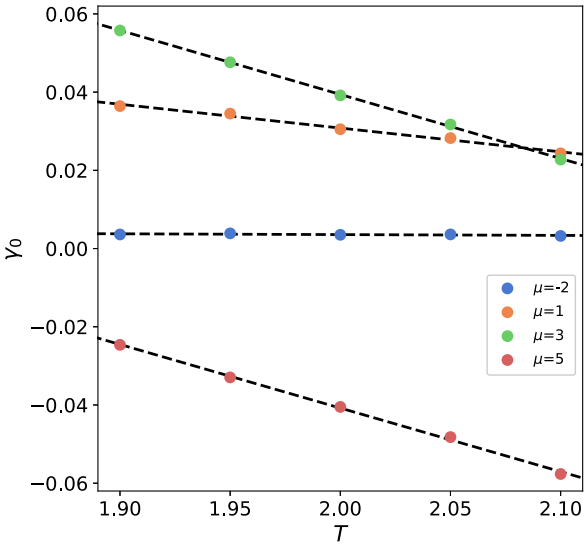

FIG. 6. Surface energy of the LJs fluid in contact with a planar wall with a WCA wall-potential, as a function of temperature. The surface energies at constant chemical potential are computed from the fitted curves in Fig. 5. The dividing surface is located at $d_{\text{wall}} = 1$.

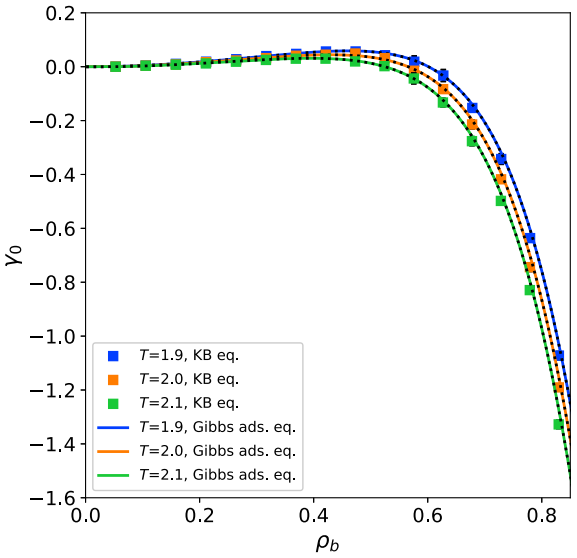

FIG. 5. Surface energy as a function of bulk density for the LJs fluid in contact with a planar wall with a WCA wall-potential. The curves fitted to the surface energy computed from Gibbs adsorption equation are displayed by the black dotted lines. The dividing surface is located at $d_{\text{wall}} = 1$.

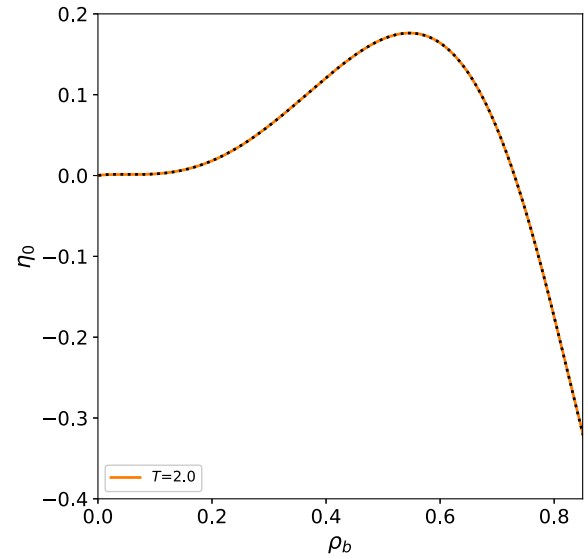

FIG. 7. Excess entropy as a function of bulk density for the LJs fluid in contact with a planar wall with a WCA wall-potential. The fitted curve is displayed by the black dotted line. The dividing surface is located at $d_{\text{wall}} = 1$.

2. *Curvature dependence of surface properties*

We will next investigate the magnitude of the curvature dependence of the adsorption, surface energy and excess entropy. Figure 8 shows the adsorption in the spherical systems and the parametrized planar-wall adsorption curve for $T = 2.0$. The data points show no observable deviation from the planar-wall curve, which suggests that the curvature dependence of the surface excess properties is very small. This is convenient, since it means that the surface properties of a planar wall can be used to describe properties of fluids confined by highly curved surfaces. The curves fitted to the adsorption of the small systems are also displayed in Fig. 8, but the deviation from the planar-wall adsorption is barely visible. Since only the two lowest densities for the spherical system with $\widetilde{R} = 5$ have well-defined bulk regions, we do not parametrize the adsorption for this size.

The first-order curvature correction of the adsorption, Γ_1, can be extracted from the adsorption as a function of $1/R$. Fig-

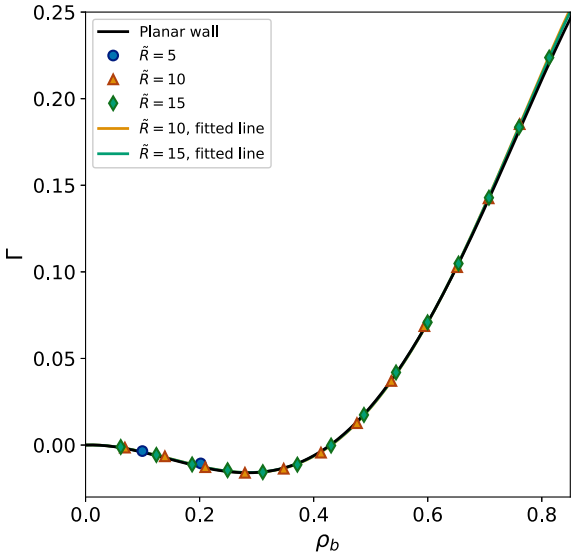

FIG. 8. Adsorption as a function of bulk density for the LJs fluid confined in small spherical systems with a WCA wall-potential. The fitted curves are displayed by the full lines. The temperature is $T = 2.0$ and the dividing surface is located at $d_{\text{wall}} = 1$.

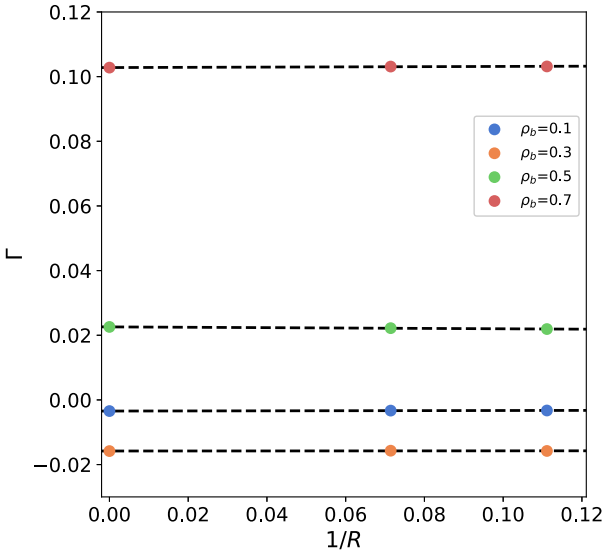

FIG. 9. Adsorption for the LJs fluid in contact with a wall with a WCA wall-potential, as a function of the inverse radius. The adsorption for the differently curved surfaces are extracted from the fitted curves in Fig. 8. The temperature is $T = 2.0$ and the dividing surface is located at $d_{\text{wall}} = 1$.

ure 9 shows the adsorption, extracted from the fitted curves, for a few selected densities as a function of inverse radius. The adsorptions for each system are extracted from the fitted curves since they must be compared at constant density, which is not represented by the discrete data points obtained directly from the simulations. The system with planar walls has infinitely large radius, which corresponds to $1/R = 0$. Figure 9 shows that the adsorption can be approximated as a first-order linear function of $1/R$, which means that a first-order

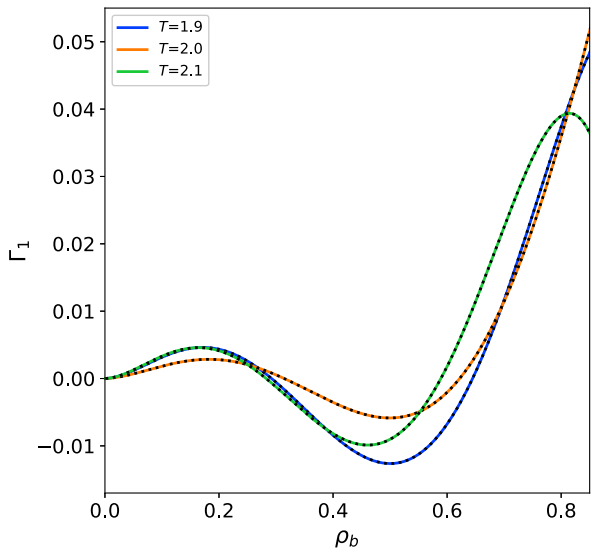

FIG. 10. First-order curvature correction of the adsorption as a function of bulk density for the LJs fluid in contact with a wall with a WCA wall-potential. The fitted curves are displayed by the black dotted lines. The dividing surface is located at $d_{\text{wall}} = 1$.

correction sufficiently describes the curvature dependence of the adsorption for the spherical systems investigated in this work. The first-order curvature corrections, extracted from the slopes of the dashed lines in Fig. 9, are displayed in Fig. 10 as functions of the bulk density.

All surface excess properties can be split into the planar-wall contribution and the curvature corrections. This means that γ_1 can be computed from Eq. (13), i.e. $\mathrm{d}\gamma_1 = \Gamma_1 \mathrm{d}\mu$, and η_1 can be computed from Eq. (14), i.e. $\eta_1 = \partial\gamma_1/\partial T|_\mu$. The first-order curvature corrections of the surface energy and excess entropy are displayed as functions of bulk density in Fig. 11 and Fig. 12 respectively. For bulk densities below $\rho_b = 0.4$, the first-order curvature corrections to all the surface excess properties have absolute values < 0.01, which indicates that the capillary approximation is excellent in this density range. The curvature corrections of the surface excess properties are parametrized with the same functions as those used for the planar-wall properties. We do not include predictions from the ideal gas in the parametrization of the curvature corrections of the surface excess properties.

V. RESULTS - VALIDATION OF THE NANO-EOS

We will next present the predictions of the Nano-EoS and compare these to the values computed directly from the MD simulations. Emphasis is placed on the internal energy and the pressure. The surface internal energy, U_s, is a combination of all the surface excess properties, which means that it provides insight on the effect of confinement on the state of the fluid. Accurate pressure predictions are key in analyzing the driving forces of transport in porous media.[31–33] Superscript "sim" refers to properties computed directly from simulations.

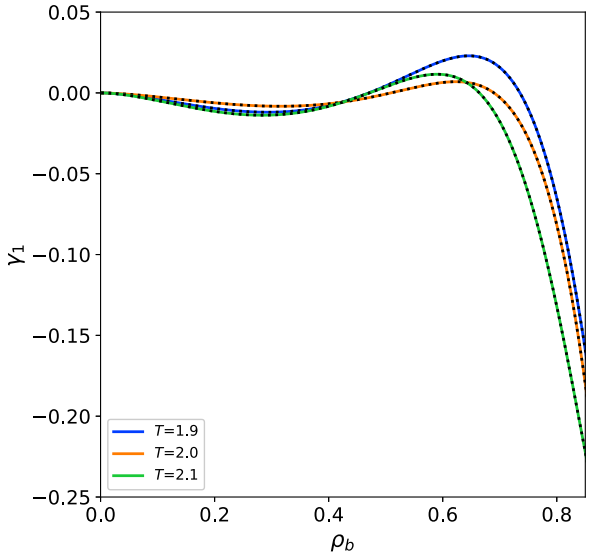

FIG. 11. First-order curvature correction of the surface energy as a function of bulk density for the LJs fluid in contact with a wall with a WCA wall-potential. The fitted curves are displayed by the black dotted lines. The dividing surface is located at $d_{\text{wall}} = 1$.

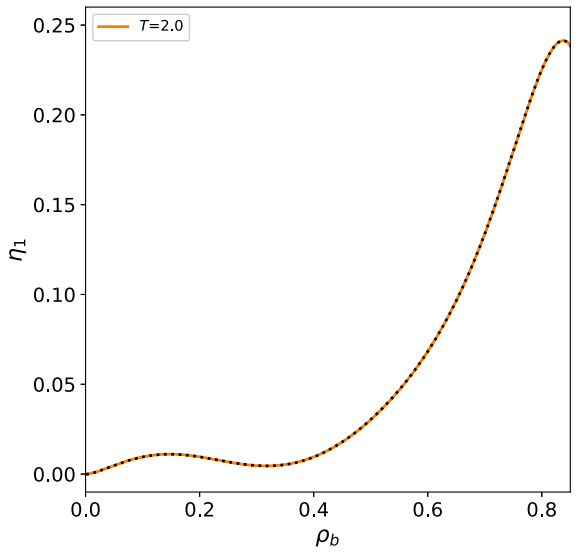

FIG. 12. First-order curvature correction of the excess entropy as a function of bulk density for the LJs fluid in contact with a wall with a WCA wall-potential. The fitted curve is displayed by the black dotted line. The dividing surface is located at $d_{\text{wall}} = 1$.

A. Pressure

The pressure computed from simulations and the predictions of the Nano-EoS are presented in Fig. 13 as functions of the total density. The large degree of overlap between the predictions from the Nano-EoS and the simulation data confirms that the pressure of the confined system can be determined as a function of T and ρ_b. The accuracy of the pressure prediction therefore mainly depends on the accuracy of the

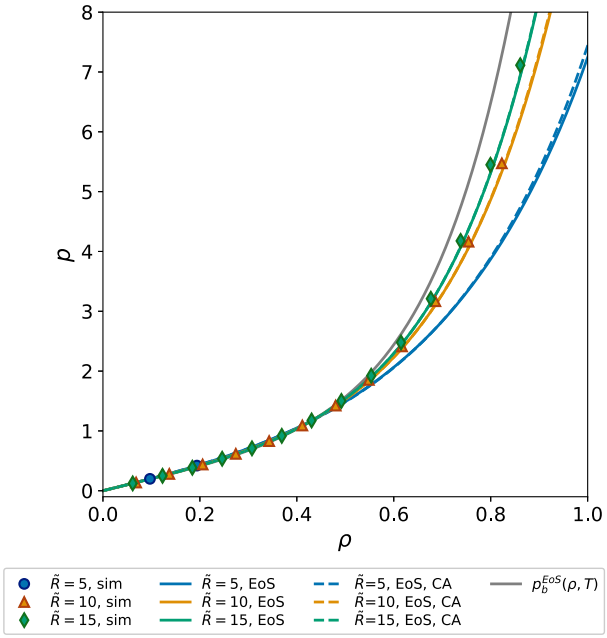

FIG. 13. Pressure as a function of the total density for the LJs fluid confined in a small spherical cavity with a WCA wall-potential. The colored full lines represent the Nano-EoS predictions including curvature corrections while the dashed lines represent the predictions of the capillary approximation. The gray line shows the pressure for a bulk system with density ρ. The temperature is $T = 2.0$ and the dividing surface is located at $d_{\text{wall}} = 1$.

predicted bulk density. The absolute error of the bulk density is the difference between predictions from the Nano-EoS and the simulation results, $\Delta\rho_{\text{b}} = |\rho_{\text{b}}^{\text{EoS}} - \rho_{\text{b}}^{\text{sim}}|$. For all system sizes and the whole range of densities considered in this work, $\Delta\rho_{\text{b}} < 0.001$.

B. Internal energy

The bulk internal energy, $U_{\text{b}}^{\text{sim}}$, is computed by multiplying the V with the internal energy density in the bulk region, which can only be computed for systems with well-defined bulk regions. Figure 14 shows the bulk internal energy normalized by the number of particles as a function of the total density. Similar to the pressure, the Nano-EoS predictions of the bulk internal energy mainly depends on the accuracy of the predicted bulk density. The accuracy of the predictions of both the pressure and the bulk internal energy therefore indicates that the parametrized adsorption presented in Sec. IV B gives an accurate representation of the adsorption in the small systems. However, the results presented in Figs. 13 and 14 give no validation of whether the curvature correction is valid beyond the range of bulk densities available from simulations.

The surface internal energy, $U_{\text{s}}^{\text{sim}} = U^{\text{sim}} - U_{\text{b}}^{\text{sim}}$, is also only accessible for systems with a well-defined bulk region. Figure 15 shows the surface internal energy per number of particles as a function of total density. Since the surface internal energy is normalized by the number of particles, the curves

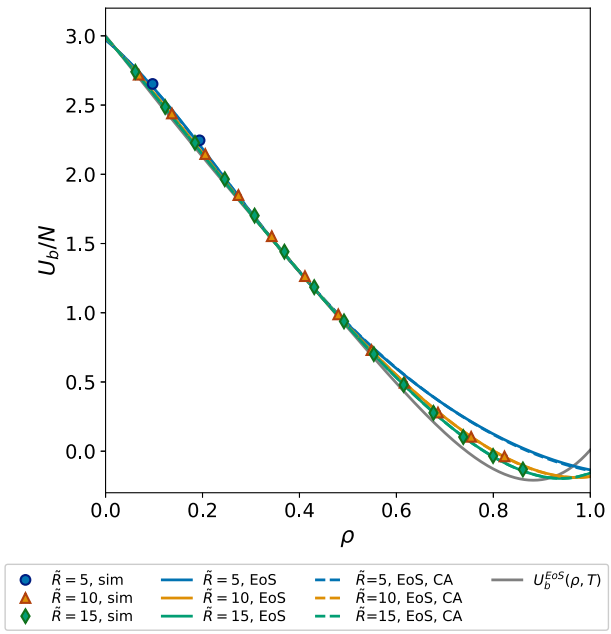

FIG. 14. Bulk internal energy (Eq. (4)) per number of particles as a function of total density for the LJs fluid confined in a small spherical cavity with a WCA wall-potential. The colored full lines represent the Nano-EoS predictions including curvature corrections while the dashed lines represent the predictions using the capillary approximation. The gray line shows the internal energy per number of particles for a bulk system with density ρ. The temperature is $T = 2.0$ and the dividing surface is located at $d_{\text{wall}} = 1$.

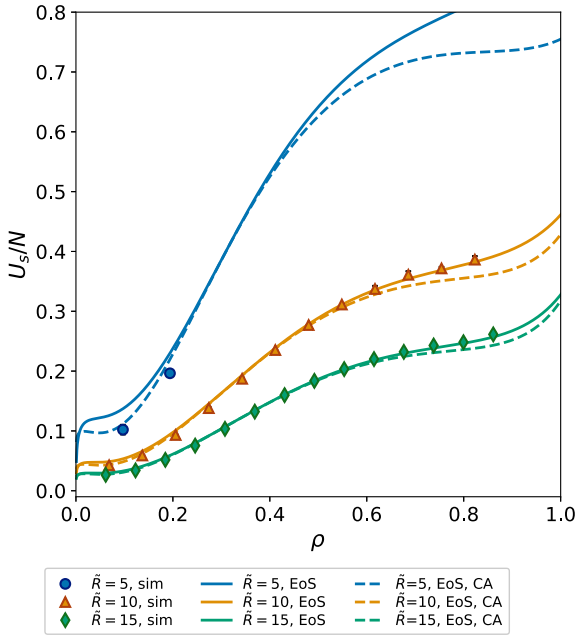

FIG. 15. surface internal energy (Eq. (5)) per number of particles as a function of total density for the LJs fluid confined in a small spherical cavity with a WCA wall-potential. The colored full lines represent the Nano-EoS predictions including curvature corrections while the dashed lines represent the predictions of the capillary approximation. The temperature is $T = 2.0$ and the dividing surface is located at $d_{\text{wall}} = 1$.

approach zero abruptly at very low densities. The large degree of overlap between the Nano-EoS predictions and the simulation results indicates that the Nano-EoS framework correctly represents the small size contributions of the confined fluid. For the two largest spherical systems at total densities below $\rho = 0.5$, the predictions of U_s^{EoS}/N from the capillary approximation are almost indistinguishable from the predictions including curvature corrections. For $\widetilde{R} = 5$, the prediction of the capillary approximation is closer to the simulation results than the prediction of the Nano-EoS including the curvature corrections. This could be due to an overestimation of the curvature correction of the surface excess properties. One factor that could lead to this overestimation is that ideal gas predictions are not included in the parametrization of the curvature corrections. The fitting procedure is therefore more sentitive to the inaccuracies of the curvature corrections computed at low densities. One likely source of the inaccuracy in the curvature correction of the surface internal energy is the excess entropy. Figures 5 and 11 show that the surface energy and has a very small temperature dependence at low densities. This means that accurate computation of the excess entropy from $\eta = \partial\gamma/\partial T|_{\mu}$ becomes challenging at low densities. It is also possible that higher order curvature corrections are needed to accurately describe the surface excess properties for a system this small.

The total internal energy, U^{sim}, is accessible for all system sizes. Figure 16 shows the internal energy per number of particles as a function of total density. The absolute error of U/N is the difference between the Nano-EoS prediction and the simulation results, $\Delta(U/N) = |(U/N)^{\text{EoS}} - (U/N)^{\text{sim}}|$. For the whole range of densities considered in this work, the absolute error is $\Delta(U/N) < 0.02$ for all system sizes. This shows that the parametrized surface excess properties and their curvature corrections extrapolate well beyond the regime of systems with well-defined bulk regions. The overlap is surprisingly good for $\widetilde{R} = 5$, given that no simulation data from this system is included in the parametrization of the surface excess properties. Similar to the predictions of the surface internal energy, the capillary approximation remains a good approximation for U^{EoS}/N for the two largest systems at total densities below $\rho = 0.5$.

VI. DISCUSSION - USE AND RANGE OF VALIDITY OF THE NANO-EOS

In the following, we discuss how the choice of dividing surface influences the applicability of the framework (Sec. VI A), the expected range of validity of the Nano-EoS (Sec. VI B), and its application to porous media (Sec. VI C).

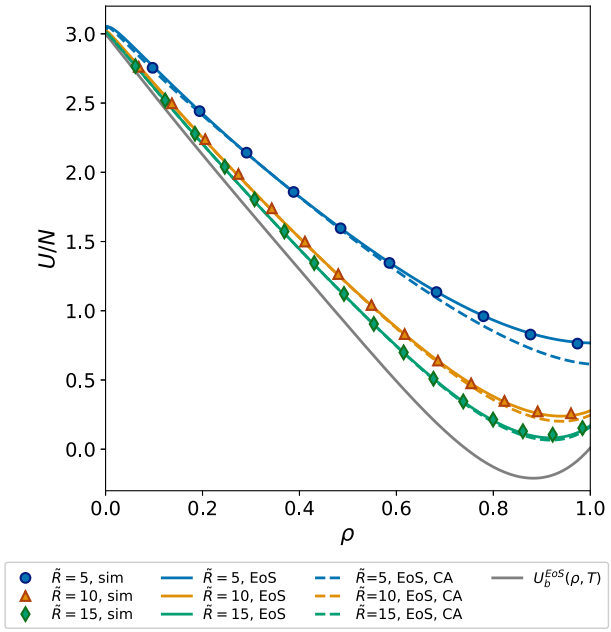

FIG. 16. Internal energy (Eq. (8)) as a function of total density for the LJs fluid confined in a small spherical cavity with a WCA wall-potential. The colored full lines represent the Nano-EoS predictions including curvature corrections while the dashed lines represent the predictions of the capillary approximation. The gray line shows the internal energy per number of particles for a bulk system with density ρ. The temperature is $T = 2.0$ and the dividing surface is located at $d_{\text{wall}} = 1$.

A. Impact of choice of dividing surface

The magnitude of both the planar-wall values and the curvature corrections of the surface excess properties depend on the choice of dividing surface.[58,59] To get more insight on this, we investigate how the choice of dividing surface impacts the accuracy of the Nano-EoS. The adsorption computed from one choice of dividing surface can easily be converted to another, arbitrary choice. We use Eqs. (22)-(26) presented in Sec. II B 2 to compute the surface excess properties for a dividing surface at $d_{\text{wall}} = 0$. This definition of system volume includes a region close to the walls with very low probability of being occupied by particles. This is clearly visible from the density profiles in Fig. 3, which are zero close to the wall for all system shapes and sizes. As a consequence, the adsorption becomes negative for the whole density range when $d_{\text{wall}} = 0$. From Eqs. (22)-(26) it is also clear that the absolute values of the planar wall contribution and the curvature correction of all surface excess properties are larger for $d_{\text{wall}} = 0$ than for $d_{\text{wall}} = 1$. This means that the capillary approximation no longer provides a satisfactory description of the surface excess properties.

The total density is also affected by the choice of dividing surface. Using $d_{\text{wall}} = 1$ is a more convenient choice since it provides a more realistic representation of the actual region that the particles are most likely to occupy. This provides more intuitive results for the adsorption and the total density, e.g. a density that is closer to the actual density in the volume occupied by particles. The bulk density, pressure and total internal energy predicted by the Nano-EoS, however, are not affected by the location of the dividing surface. Figures showing all surface excess properties, their curvature corrections, the different internal energy contributions and the pressure for $d_{\text{wall}} = 0$ at $T = 2.0$ are presented in supplementary material. Many other choices for dividing surface exist, probably including more optimal choices than $d_{\text{wall}} = 1$, but we do not further investigate the choice of dividing surface here.

B. Expected accuracy and range of validity

In the Nano-EoS framework, the effect of confinement is included in the confined fluid's internal energy. For ensemble equivalent systems, the energy state functions for various ensembles are accessible from Legendre transformations of the internal energy. When the energy state function of a system is known, the full thermodynamic description of that system is accessible. We therefore expect the accuracy of the predictions of the entropy, enthalpy and energy state functions such as Helmholtz energy or Gibbs energy to be comparable to the accuracy of the internal energy predictions presented in this work. The intensive properties of the confined fluid depend on the bulk density and the temperature. The accuracy of the predictions of intensive properties, such as the chemical potential and compressibility, is therefore expected to be comparable to the accuracy of the pressure predictions presented in this work.

In this work, we consider pure fluids, but extension to mixtures is possible. The framework can also be extended to other geometries by including the appropriate curvature corrections, line contributions and edge contributions.[39] However, if the interactions between the wall and the particles cannot be approximated by a smooth potential, more complex shape effects e.g. inaccessible regions or energetically favored hot-spots can arise, which are not so easily captured by size and shape corrections.[13] Such complex shape effects only come into play when the confined system is small enough. This lower size limit depends on both the inter-particle interactions and the wall-particle interactions. Other effects that can occur for very small systems are surface-surface interactions, which lead to disjoining pressure effects.[60] We expect that further modifications of the framework and methodology are necessary for the Nano-EoS to extrapolate well to these situations.

An alternative framework for thermodynamics of small systems is the nanothermodynamics developed by Hill.[28] Instead of introducing specific contributions from e.g. the surface or the curvature, Hill's formalism provides a general framework for thermodynamics of a system influenced by small size effects. For confined fluids, the thermodynamic functions suggested by Hill therefore provide descriptions of the whole system, with bulk and surface combined. A key part of the derivation of Hill's nanothermodynamics is that each thermodynamic ensemble is considered separately. As a consequence, new ensemble-specific properties that are unique to small system arise. Hill showed how his framework can be

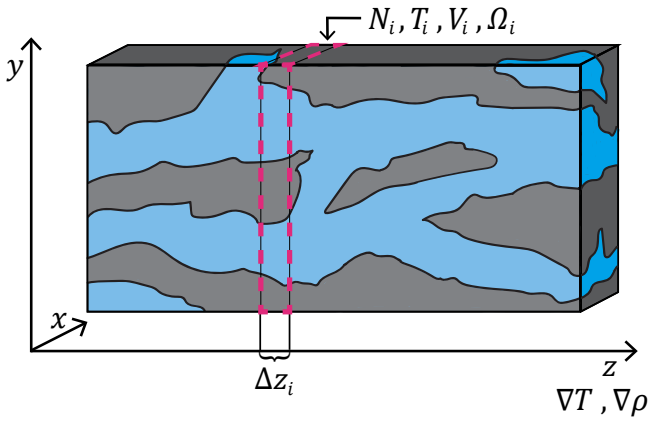

FIG. 17. Illustration of a fluid (blue) in a porous media (gray). When local equilibrium is assumed in the REV (red dash), the Nano-EoS can be used to compute the state of the fluid for the number of particles, N, and temperature T. In the control volume, the volume of the confined fluid is the blue region. The surface excess properties represent to the area corresponding to the interface between the blue and gray region. The exact values of V and Ω depend on the dividing surface.

applied to spherical droplets in vapor in a way that does not require a dividing surface. By introducing a dividing surface, the formalism by Hill can be connected to Gibbs' description.[28] A possibility for future work is therefore to compare Hill's formalism with the framework presented here. This can provide further insight into the ensemble-specific properties introduced by Hill.

C. Use of the Nano-EoS in porous media

For systems with LJs particles in contact with a spherical surface with a WCA wall-potential at $T = 2.0$, the functions for the surface excess properties provided in the supplementary material can be used directly to predict properties of systems in equilibrium. A possible application of the Nano-EoS is to predict thermodynamic properties in porous media. To explain how the Nano-EoS can be used for this purpose, we use the porous medium depicted in Fig. 17 as an example. This example represents a single-component system with a gradient in thermodynamic properties such as T and ρ in the z-direction, but not in the x- and y-directions.

We consider a slab of width Δz_i, which we refer to as a representative elementary volume (REV). Across the REV, the gradients in thermodynamic properties are sufficiently small to invoke the assumption of *local equilibrium*. Local equilibrium in this context means that the thermodynamic properties of the fluid in the slab can be described by the equations elaborated in Sec. II. This includes thermal and chemical equilibrium between the fluid, the solid and the surface between these two phases within the slab. Discussions of criteria for defining a REV in a porous medium can be found in Refs.[61,62]

We assume that the average number of particles, N_i, and the temperature, T_i, inside the slab are available, which is usually the case for porous media examined by molecular simulations. After defining the dividing surface between the fluid and solid, the volume, V_i, and the area, Ω_i within the slab as well as the average curvature can be computed. With these variables available, combined with the assumption of local equilibrium in the REV, thermodynamic properties such as the local pressure and chemical potential can be computed by using the algorithm described in Fig. 2. Necessary inputs are a bulk-EoS and a function for the adsorption. Use of the framework as presented in Sec. II assumes that line and edge contributions to the internal energy can be neglected. The results shown in Sec. V indicate that at least for some types of wall-particle interactions, the capillary approximation works well such that the influence of curvature can be neglected.

VII. CONCLUSIONS

Equations of state (EoS) provide a compact way to describe the thermodynamic state of a fluid. For bulk systems, the thermodynamic state of the fluid can be predicted from an EoS when the temperature, mass density and composition are provided. When a fluid is confined in a small enough space, its properties will deviate from bulk behavior due to the interactions between the fluid particles and the wall. Hence, for fluids under confinement, the impact of the enclosing surface on the fluid properties must be included in the EoS. In this work, we have presented a theoretical framework that describes the thermodynamic state of a confined fluid at equilibrium. The framework applies to a wide variety of inter-particle interactions, wall-fluid interactions and system geometries, and is independent of the system's ensemble. When the underlying physical description of the fluid is provided, the framework presented represents an EoS for confined fluids. We refer to the proposed EoS for confined fluids as the "Nano-EoS". In the Nano-EoS, the description of the total confined system is split into a bulk phase and an excess surface phase. The properties of the bulk phase are provided by a bulk-EoS and the properties of the surface phase are described by Gibbs' framework for excess variables. For equilibrium systems, these two phases have the same temperature and chemical potential. Intensive properties of the total system such as chemical potential and pressure are therefore accessible from the properties of the bulk phase at ρ_b and T.

We have demonstrated the application of the Nano-EoS for a LJs fluid in contact with spherical surface with a WCA wall-potential. For this system, the Nano-EoS predicts values for the internal energy and pressure nearly within the accuracy of the values computed directly from MD simulations. Since the framework is ensemble independent, the energy state functions for any ensemble can be computed from Legendre transformations of the internal energy. Potential applications are therefore prediction of the properties in control volumes at local equilibrium in a larger, non-equilibrium system.

The location of the dividing surface determines the volume of the system and for curved surfaces, it also determines the surface area. The magnitude of the surface excess properties are therefore highly dependent on the choice

of dividing surface. We have investigated two choices of dividing surface, one located at the origin of the wall potential ($d_{\text{wall}} = 0$) and one located at the collision diameter of the wall potential ($d_{\text{wall}} = 1$). We found that a dividing surface located at $d_{\text{wall}} = 1$ returns lower absolute values for surface excess properties and their curvature dependence than $d_{\text{wall}} = 0$. Choosing a dividing surface that gives a small curvature dependence is convenient since it means that properties of highly curved surfaces can be accurately described by the properties of a planar surface. In other words, the so-called capillary approximation becomes increasingly valid.

In the low-density limit, the thermodynamic properties of a confined fluid with interacting particles approach those of a confined ideal gas. We have therefore derived exact analytical expressions for the surface excess properties of a confined ideal gas. The surface properties of the ideal gas are included in the Nano-EoS in order to ensure consistent extrapolation to the low-density limit. However, for confined fluids at low densities, the ideal gas predictions can also be used as an independent EoS to predict fluid properties.

ACKNOWLEDGMENTS

This work was supported by the Research Council of Norway (Grant No. 275754). Thanks to the Center of Excellence funding scheme of the Research Council of Norway, (Grant No. 262644), PoreLab. Computational resources are provided by UNINETT Sigma2 - The National Infrastructure for High Performance Computing and Data Storage in Norway (Grant No. NN9414k). The authors greatly appreciate discussions with Michael Rauter, Dick Bedeaux, Signe Kjelstrup and Bjørn Hafskjold.

AUTHOR DECLARATIONS

The authors have no conflicts to disclose.

DATA AVAILABILITY STATEMENT

The LAMMPS simulation input files and text files containing the coefficients for the parametrized curves of the surface excess properties are openly available in Zenodo at https://doi.org/10.5281/zenodo.6478153.

[1]A. V. Neimark and K. G. Kornev, "Classification of equilibrium configurations of wetting films on planar substrates," Langmuir. **16**, 5526–5529 (2000).
[2]A. V. Neimark, P. I. Ravikovitch, and A. Vishnyakov, "Inside the hysteresis loop: Multiplicity of internal states in confined fluids," Phys. Rev. E. **65**, 031505 (2002).
[3]T. Horikawa, D. D. Do, and D. Nicholson, "Capillary condensation of adsorbates in porous materials," Adv. Colloid Interface Sci. **169**, 40–58 (2011).
[4]T. Hiratsuka, H. Tanaka, and M. T. Miyahara, "Comprehensive modeling of capillary condensation in open-ended nanopores: Equilibrium, metastability, and spinodal," J. Phys. Chem. C. **121**, 26877–26886 (2017).
[5]L. Liu, S.-H. Chen, A. Faraone, C.-W. Yen, and C.-Y. Mou, "Pressure Dependence of Fragile-to-Strong Transition and a Possible Second Critical Point in Supercooled Confined Water," Phys. Rev. Lett. **95**, 117802 (2005).
[6]J. K. Brennan, T. J. Bandosz, K. T. Thomson, and K. E. Gubbins, "Water in porous carbons," Colloids Surf. **187-188**, 539–568 (2001).
[7]X.-Q. Chu, K.-H. Liu, M. S. Tyagi, C.-Y. Mou, and S.-H. Chen, "Low-temperature dynamics of water confined in a hydrophobic mesoporous material," Phys. Rev. E. **82**, 020501 (2010).
[8]Y.-X. Yu, F.-Q. You, Y. Tang, G.-H. Gao, and Y.-G. Li, "Structure and Adsorption of A Hard-Core Multi-Yukawa Fluid Confined in A Slitlike Pore: Grand Canonical Monte Carlo Simulation and Density Functional Study," J. Phys. Chem. B. **110**, 334–341 (2006).
[9]B. Peng and Y.-X. Yu, "A Density Functional Theory for Lennard-Jones Fluids in Cylindrical Pores and Its Applications to Adsorption of Nitrogen on MCM-41 Materials," Langmuir. **24**, 12431–12439 (2008).
[10]Y.-X. Yu, "A novel weighted density functional theory for adsorption, fluid-solid interfacial tension, and disjoining properties of simple liquid films on planar solid surfaces," J. Chem. Phys. **131**, 024704 (2009).
[11]L.-Y. Wang, F. Gu, H.-J. Wang, and Z.-L. Sun, "Pressure Profile for an Associating Lennard-Jones Fluid Confined in a Spherical Cavity," J. Phys. Chem. B. **121**, 2142–2152 (2017).
[12]B. R. Didar and I. Y. Akkutlu, "Pore-size Dependence of Fluid Phase Behavior and Properties in Organic-Rich Shale Reservoirs," SPE International Symposium on Oilfield Chemistry. (2013).
[13]H. Cárdenas and E. A. Müller, "How does the shape and surface energy of pores affect the adsorption of nanoconfined fluids?" AIChE J. **67**, e17011 (2021).
[14]V. Bråten, D. Bedeaux, Ø. Wilhelmsen, and S. K. Schnell, "Small size effects in open and closed systems: What can we learn from ideal gases about systems with interacting particles?" J. Chem. Phys. **155**, 244504 (2021).
[15]I. Urrutia, "Three hard spheres in a spherical cavity," J. Chem. Phys. **135**, 024511 (2011).
[16]A. Aasen, M. Hammer, G. Skaugen, J. P. Jakobsen, and Ø. Wilhelmsen, "Thermodynamic models to accurately describe the PVTxy-behavior of water / carbon dioxide mixtures," Fluid Phase Equilib. **442**, 125–139 (2017).
[17]V. Koulocheris, V. Louli, E. Panteli, S. Skouras, and E. Voutsasa, "Modelling of elemental mercury solubility in natural gas components," Fuel. **233**, 558–564 (2018).
[18]G. J. Zarragoicoechea and V. A. Kuz, "van der Waals equation of state for a fluid in a nanopore," Phys. Rev. E. **65**, 021110 (2002).
[19]G. J. Zarragoicoechea and V. A. Kuz, "Critical shift of a confined fluid in a nanopore," Fluid Phase Equilib. **220**, 7–9 (2004).
[20]L. Travalloni, M. Castier, F. W. Tavares, and S. I. Sandler, "Thermodynamic modeling of confined fluids using an extension of the generalized van der Waals theory," Chem. Eng. Sci. **65**, 3088–3099 (2010).
[21]L. Travalloni, M. Castier, F. W. Tavares, and S. I. Sandler, "Critical behavior of pure confined fluids from an extension of the van der Waals equation of state," J. Supercrit. Fluids. **55**, 455–461 (2010).
[22]Ø. Wilhelmsen, A. Aasen, G. Skaugen, P. Aursand, A. Austegard, E. Aursand, M. Gjennestad, H. Lund, G. Linga, and M. Hammer, "Thermodynamic Modeling with Equations of State: Present Challenges with Established Methods," Ind. Eng. Chem. Res. **56**, 3503–3515 (2017).
[23]M. Holovko, T. Patsahan, and W. Dong, "Fluids in random porous media: Scaled particle theory," Pure Appl. Chem. **85**, 115–133 (2012).
[24]M. F. Holovko, T. M. Patsahan, and V. I. Shmotolokha, "What is liquid in random porous media: the Barker-Henderson perturbation theory," Condens. Matter Phys. **18**, 13607 (2015).
[25]T. V. Hvozd, Y. V. Kalyuzhnyi, and P. T. Cummings, "Phase Equilibria of Polydisperse Square-Well Chain Fluid Confined in Random Porous Media: TPT of Wertheim and Scaled Particle Theory," J. Phys. Chem. B. **122**, 5458–5465 (2018).
[26]A. Nelson, Y. Kalyuzhnyi, T. Patsahan, and C. McCabe, "Liquid-vapor phase equilibrium of a simple liquid confined in a random porous media: Second-order Barker-Henderson perturbation theory and scaled particle theory," J. Mol. Liq. **300**, 112348 (2020).
[27]D. Bedeaux, S. Kjelstrup, and S. K. Schnell, *Nanothermodynamics. General theory* (Porelab publisher, 2020).
[28]T. L. Hill, *Thermodynamics of Small Systems* (Dover Publications, New York, 1994).

[29]E. Bering, S. Kjelstrup, D. Bedeaux, J. M. Rubi, and A. S. de Wijn, "Entropy Production beyond the Thermodynamic Limit from Single-Molecule Stretching Simulations," J. Phys. Chem. B. **124**, 8909–8917 (2020).

[30]E. Bering, D. Bedeaux, S. Kjelstrup, A. S. de Wijn, I. Latella, and J. M. Rubi, "A Legendre–Fenchel Transform for Molecular Stretching Energies," Nanomaterials. **10** (2020).

[31]O. Galteland, D. Bedeaux, B. Hafskjold, and S. Kjelstrup, "Pressures Inside a Nano-Porous Medium. The Case of a Single Phase Fluid," Front. Phys. **7**, 60 (2019).

[32]M. T. Rauter, O. Galteland, M. Erdős, O. A. Moultos, T. J. H. Vlugt, S. K. Schnell, D. Bedeaux, and S. Kjelstrup, "Two-Phase Equilibrium Conditions in Nanopores," Nanomaterials. **10** (2020).

[33]O. Galteland, D. Bedeaux, and S. Kjelstrup, "Nanothermodynamic Description and Molecular Simulation of a Single-Phase Fluid in a Slit Pore," Nanomaterials. **11** (2021).

[34]S. K. Schnell, T. J. H. Vlugt, J.-M. Simon, D. Bedeaux, and S. Kjelstrup, "Thermodynamics of small systems embedded in a reservoir: a detailed analysis of finite size effects," Mol. Phys. **110**, 1069–1079 (2012).

[35]B. A. Strøm, J.-M. Simon, S. K. Schnell, S. Kjelstrup, J. He, and D. Bedeaux, "Size and shape effects on the thermodynamic properties of nanoscale volumes of water," Phys. Chem. Chem. Phys. **19**, 9016–9027 (2017).

[36]V. Bråten, Ø. Wilhelmsen, and S. K. Schnell, "Chemical Potential Differences in the Macroscopic Limit from Fluctuations in Small Systems," J. Chem. Inf. Model. **61**, 840–855 (2021).

[37]J. W. Gibbs, *The Scientific Papers of J. Willard Gibbs* (Ox Bow Press, London, 1993).

[38]R. C. Tolman, "The Effect of Droplet Size on Surface Tension," J. Chem. Phys. **17**, 333–337 (1949).

[39]W. Helfrich, "Elastic Properties of Lipid Bilayers: Theory and Possible Experiments," Zeitschrift für Naturforschung C. **28**, 693–703 (1973).

[40]A. Aasen, E. M. Blokhuis, and Ø. Wilhelmsen, "Tolman lengths and rigidity constants of multicomponent fluids: Fundamental theory and numerical examples," J. Chem. Phys. **148**, 204702 (2018).

[41]A. Aasen, D. Reguera, and Ø. Wilhelmsen, "Curvature corrections remove the inconsistencies of binary classical nucleation theory," Phys. Rev. Lett. **124**, 045701 (2020).

[42]I. E. Paganini, R. L. Davidchack, B. B. Laird, and I. Urrutia, "Properties of the hard-sphere fluid at a planar wall using virial series and molecular-dynamics simulation," The Journal of Chemical Physics **149**, 014704 (2018).

[43]J. G. Kirkwood and F. P. Buff, "The Statistical Mechanical Theory of Surface Tension," J. Chem. Phys. **17**, 338–343 (1949).

[44]T. Ikeshoji, B. Hafskjold, and H. Furuholt, "Molecular-level Calculation Scheme for Pressure in Inhomogeneous Systems of Flat and Spherical Layers," Mol. Sim. **29**, 101–109 (2003).

[45]Y. Long, M. Śliwińska Bartkowiak, H. Drozdowski, M. Kempiński, K. A. Phillips, J. C. Palmer, and K. E. Gubbins, "High pressure effect in nanoporous carbon materials: Effects of pore geometry," Colloids Surf. A: Physicochem. Eng. Asp. **437**, 33–41 (2013).

[46]Z. Sun, Y. Kang, and J. Zhang, "Density functional study of pressure profile for hard-sphere fluids confined in a nano-cavity," AIP Advances. **4**, 031308 (2014).

[47]K. Shi, E. E. Santiso, and K. E. Gubbins, "Can we define a unique microscopic pressure in inhomogeneous fluids?" J. Chem. Phys. **154**, 084502 (2021).

[48]J.-P. Hansen and I. R. McDonald, *Theory of simple liquids: with applications to soft matter* (Academic press, 2013).

[49]S. Plimpton, "Fast Parallel Algorithms for Short-Range Molecular Dynamics," J. Comp. Phys. **117**, 1–19 (1995).

[50]B. L. Holian and D. J. Evans, "Shear viscosities away from the melting line: A comparison of equilibrium and nonequilibrium molecular dynamics," J. Chem. Phys. **78**, 5147–5150 (1983).

[51]B. Hafskjold, K. P. Travis, A. B. Hass, M. Hammer, A. Aasen, and Ø. Wilhelmsen, "Thermodynamic properties of the 3D Lennard-Jones/spline model," Mol. Phys. **117**, 3754–3769 (2019).

[52]J. D. Weeks, D. Chandler, and H. C. Andersen, "Role of Repulsive Forces in Determining the Equilibrium Structure of Simple Liquids," J. Chem. Phys. **54**, 5237–5247 (1971).

[53]T. van Westen and J. Gross, "Accurate thermodynamics of simple fluids and chain fluids based on first-order perturbation theory and second virial coefficients: uv-theory," J. Chem. Phys. **155**, 244501 (2021).

[54]T. van Westen, M. Hammer, B. Hafskjold, A. Aasen, J. Gross, and Ø. Wilhelmsen, "Perturbation theories for fluids with short-ranged attractive forces: A case study of the Lennard-Jones spline fluid," J. Chem. Phys. **156**, 104504 (2022).

[55]SINTEF, "Thermopack," `https://github.com/SINTEF/thermopack` (2022).

[56]F. Heidari, T. Keshavarzi, and G. Mansoori, "Attractive energy contribution to nanoconfined fluids behavior: the normal pressure tensor," Microfluid. Nanofluid. **10**, 899–906 (2011).

[57]A. Helmi and E. Keshavarzi, "The role of concavo-convex walls of a nanopore on the density profile, adsorption, solvation force, and capillary condensation of confined fluids: A DFT study," Chem. Phys. **433**, 67–75 (2014).

[58]I. Urrutia, "Bending rigidity and higher-order curvature terms for the hard-sphere fluid near a curved wall," Phys. Rev. E. **89**, 032122 (2014).

[59]A. Reindl, M. Bier, and S. Dietrich, "Implications of interface conventions for morphometric thermodynamics," Phys. Rev. E. **91**, 022406 (2015).

[60]M. A. Gjennestad and Ø. Wilhelmsen, "Thermodynamic stability of volatile droplets and thin films governed by the disjoining pressure in open and closed containers," Langmuir. (2020).

[61]S. Whitaker, "Flow in porous media I: A theoretical derivation of Darcy's law," Transp. Porous Med. **1**, 3–25 (1986).

[62]O. Galteland, M. T. Rauter, M. S. Bratvold, T. T. Trinh, D. Bedeaux, and S. Kjelstrup, "Local thermodynamic description of isothermal single-phase flow in porous media," arXiv preprint arXiv:2203.02334 (2022).